THE JOURNAL OF PHYSICAL CHEMISTRY Letters

Letter

pubs.acs.org/JPCL

Microalloying Boron Carbide with Silicon to Achieve Dramatically Improved Ductility

Qi An and William A. Goddard, III*

Materials and Process Simulation Center (Mail Code 139-74), California Institute of Technology, 1200 East California Boulevard, Pasadena, California 91125, United States

ABSTRACT: Boron carbide (B_4C) is a hard material whose value for extended engineering applications such as body armor; is limited by its brittleness under impact. To improve the ductility while retaining hardness, we used density functional theory to examine modifying B_4C ductility through microalloying. We found that replacing the CBC chain in B_4C with Si−Si, denoted as $(B_{11}C_p)$−Si_2, dramatically improves the ductility, allowing a continuous shear to a large strain of 0.802 (about twice of B_4C failure strain) without brittle failure. Moreover, $(B_{11}C)$−Si_2 retains low density and high hardness. This ductility improvement arises because the Si−Si linkages enable the icosahedra accommodate additional shear by rotating instead of breaking bonds.

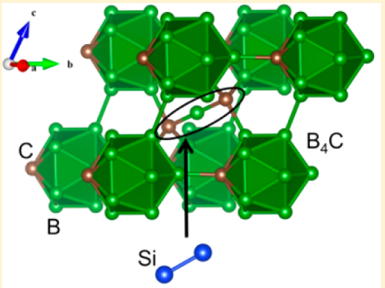

Substitute C-B-C chain with Si_2 pair; leading to lower density, and increased ductility.

SECTION: Plasmonics, Optical Materials, and Hard Matter

Superhard materials, such as diamond, cubic boron nitride, and boron carbide (B_4C), exhibit many valuable properties: high melting temperature, large compression strength, chemical inertness, and high thermal conductivity, making them of practical importance for science and engineering applications.[1−6] However, they are brittle with low fracture toughness. This serious flaw prevents many engineering applications, in particular involving extreme environments of high stress and hypervelocity impact. Efforts to improve the fracture toughness include designing functional microstructures and forming porous structures.[7−10] However, improvement of fracture toughness is often at the expense of hardness and wear resistance. To achieve new materials for extended engineering applications, we want to redesign hard materials to be ductile without sacrificing these properties.

Boron carbide (B_4C) is extremely hard (Vickers hardness 30 GPa), although less hard than diamond (Vickers hardness 115 GPa) and cubic boron nitride (Vickers hardness 76 GPa). Because of its novel properties of high hardness, low density, and abrasion resistance, B_4C is widely used in refractory applications, abrasive powders, and body armor and as a neutron radiation absorbent.[11−21] However, B_4C fractures easily just above the Hugoniot elastic limit (HEL, ∼20 GPa) at hypervelocity impact and high pressures.[22−25] This low fracture toughness results from formation of local amorphization shear bands,[16,26−28] for which the atomistic mechanism has been elucidated from combining experimental and computational studies.[16−18,27−30] In particular, we examined the response of B_4C to shear along 11 slip systems and found that the slip system with the lowest shear strength, $(01\bar{1}1)/\langle\bar{1}101\rangle$, leads to a unique plastic deformation before failure in which a boron−carbon bond between neighboring icosahedral clusters breaks to form a carbon lone pair (Lewis base) on the C within the icosahedron.[30] Further shear then leads this Lewis base C to form a new bond with the Lewis acidic B in the middle of a CBC chain. This then initiates destruction of the icosahedron and subsequent failure.

We take the hard material B_4C as the prototype and examine how to improve its ductility through microalloying. Using the PBE flavor of density functional theory (DFT), we examined the changes of mechanical properties including ductility, density, and hardness by modifying the CBC chains connecting the icosahedra in B_4C. We first assessed the ductility of various modified structures using the empirical criterion that the ratio of the bulk modulus to the shear modulus (B/G) should be better than B_4C (>1.20). Then, we selected the best cases with improved ductility, low density, and high hardness and sheared them along the amorphous slip system in B_4C to examine the shear failure model and ductility of new systems.

The description of the structure and bonding of B_4C from previous studies[13,30,31] is as follows. Figure 1a shows the unit cell of B_4C, which belongs to the rhombohedral space group ($R\bar{3}m$). It consists of one icosahedron per cell with six lattice vertices (denoted as e for equatorial site) that each connect to a different icosahedron through a three atom chain along the $\langle 111\rangle_r$ direction where r represents rhombohedra.[13,31] In addition, each icosahedron makes direct connections to the other six neighboring icosahedra through six lattice vertices denoted as p for polar site. The chemical formula B_4C used to refer to boron carbide is understood to denote a range of stoichiometries because the locations of carbon atoms are not determined experimentally. DFT predicts that the ground-state

Received: October 27, 2014
Accepted: November 18, 2014
Published: November 18, 2014

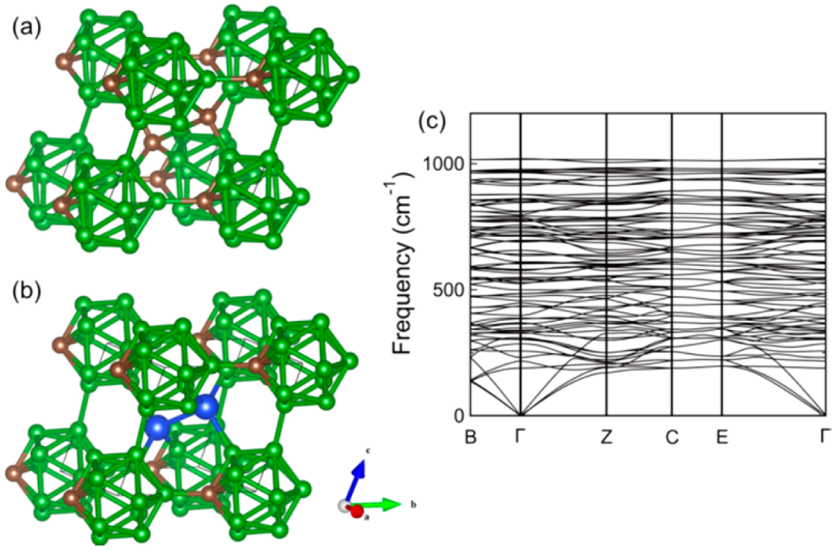

Figure 1. (a) $(B_{11}C_p)$CBC ground-state structure for B_4C (rhombohedral representation); (b) Si microalloyed structure, $(B_{11}C_p)-Si_2$; and (c) predicted phonon spectrum for $(B_{11}C_p)-Si_2$. Here boron is green, carbon is sienna, and silicon is blue.

structure is $(B_{11}C_p)$CBC.[13,30] The CBC three-atom chain has two two-center−two-electron (2c−2e) sigma bonds from the central B of the chain to the chain carbon atoms, while each chain carbon also makes three 2c−2e bonds to boron atoms of three adjacent icosahedra. Thus, the middle boron in the CBC chain has one net positive formal charge. As a result, the $(B_{11}C_p)$ cage has 26 e involved in intraicosahedral bonding, stabilizing the icosahedral structure (Wade's rule).[32,33]

To examine how microalloying might modify the mechanical properties, we start by modifying the chain structures connecting icosahedra. We tried many systems, but the most interesting is the modified structure in which a Si−Si pair replaces the CBC chain, leading to the chemical formula $(B_{11}C_p)-Si_2$, as shown in Figure 1b. The ductility improvement is due to changes in the deformation mechanism upon microalloying with Si.

Several alloyed boron materials retaining the icosahedral motif have been synthesized experimentally, including B_4C, $B_{12}P_2$, and B_6O. These are formed by inserting a three-atom or two-atom chain unit into six of inter icosahedral bonds of alpha boron.[31] Our studies of the deformations of B_4C suggested that the interaction between chain and cage plays an essential role in deconstruction of the structures.[30] Thus, we examined how the mechanical properties change upon modifying the CBC chain in $(B_{11}C_p)$CBC structure. In particular, we replaced the C−B−C chain with various two-atom pairs or single atoms, such as Si−Si, N−N, S−S, P−P, CH_2C, and S. We also included the high energy B_4C structure (B_{12})CCC (1.09 eV/unit cell higher in energy) and the boron-rich boron carbide (B_{12})CBC.

The calculated densities, ductility indexes, and hardness are shown in Table 1. We find that $(B_{11}C_p)-Si_2$ has the best ductility index of 1.59 compared with 1.20 for B_4C and 1.03 for α-boron. It also has a low density of 2.454 g/cm^3 (2.7% lower than the 2.523 g/cm^3 of $(B_{11}C_p)$CBC. The hardness decreases slightly to 27.8 GPa compared with 31.7 GPa for $(B_{11}C_p)$CBC. The other new structures with improved ductility and lower density include (B_{12})CCC, (B_{12})CBC, and $(B_{11}C_p)CH_2C$, which have B/G equal to 1.26, 1.37, and 1.27, respectively. We observed that $(B_{11}C_p)$S has a density and ductility, similar to $(B_{11}C_p)-Si_2$, but its decreased hardness of 21.4 GPa makes it less promising.

Table 1. Predicted Density, Ductility Index, and Knoop Hardness of Materials Modified from Boron Carbide

compound	density (g/cm^3)	B/G (ductility index)	hardness (GPa)
$(B_{11}C_p)$(C−B−C)	2.523	1.20	31.7
$(B_{11}C_p)$(Si−Si)	2.454	1.59	27.8
(B_{12})(C−B−C)	2.439	1.37	30.2
(B_{12})(C−C−C)	2.470	1.26	41.4
$(B_{11}C_p)$(NN)	2.605	1.11	27.0
$(B_{11}C_p)$S	2.540	1.53	21.4
$(B_{11}C_p)$(SS)	2.651	1.43	23.6
$(B_{11}C_p)$(P−P)	2.642	1.00	24.0
$(B_{11}C_p)$(C−H H−C)	2.404	1.27	33.9

Because the B/G criterion indicates that $(B_{11}C_p)-Si_2$ has the best ductility, we examined the stability of this new structure. The PBE predicted structure has the space group of *Cm* with primitive cell parameters of a = 5.363 Å, c = 5.099 Å, α = 109.207°, and γ = 70.622°. The predicted phonon spectrum (Figure 1c) shows that the Hessian has no negative eigenvalues, indicating that this structure is dynamically stable. The B/G criterion is only an empirical rule to estimate ductility for metals.[34] To prove that the new structure $(B_{11}C_p)-Si_2$ has good ductility and to validate the B/G criterion, we sheared the system along the amorphous slip system of $(01\bar{1}1)/<\bar{1}101>$ found in B_4C.[29,30] We also sheared the (B_{12})CCC and (B_{12})CBC structures expected to have improved ductility.

Figure 2 shows the stress−strain curves for these three systems along with $(B_{11}C_p)$CBC. These results show that the failure strain is 0.348 for $(B_{11}C_p)$CBC, while (B_{12})CCC and (B_{12})CBC lead to a failure strain of 0.381 and 0.348. The ideal shear strengths for (B_{12})CCC and (B_{12})CBC are 51.0 and 45.8 GPa compared with 39.0 GPa for $(B_{11}C_p)$CBC. This illustrates that modifying the chain structures can improve the ductility and that the B/G criterion is useful for predicting changes in ductility. However, current methods of synthesis cannot control the fractions of carbon in the chains and icosahedra, and current materials may already have grains or regions with these more favorable materials. Of course, the grain boundaries may play an important role in ductility, a factor not considered here.

dx.doi.org/10.1021/jz5022697 | *J. Phys. Chem. Lett.* 2014, 5, 4169−4174

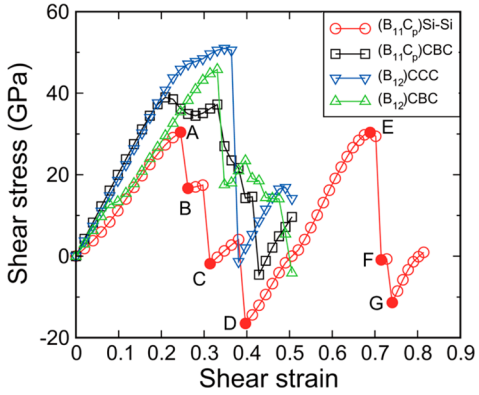

Figure 2. Stress−strain relation of various structures shearing along the $(01\bar{1}1)/<\bar{1}101>$ amorphous slip system of B_4C. The ground-state $(B_{11}C_p)$CBC fails catastrophically at a strain of 0.348. The less stable structure (B_{12})CCC and the boron-rich structure (B_{12})CBC fail catastrophically at strains of 0.348 and 0.381. The ductile structure $(B_{11}C_p)-Si_2$ shows structural changes at strains of 0.397 and 0.741 without brittle failure. The filled circles represent the key structural steps examined in Figures 3 and 4

We next consider that a system such as $(B_{11}C_p)-Si_2$. The predicted stress−strain curve for $(B_{11}C_p)-Si_2$ (Figure 2) shows a plastic ductile behavior. That is, it is elastic until a shear of 0.245, but instead of failing by amorphous shear as in B_4C, we see the stress continuous increase after strains of 0.397 and then decrease at the strain of 0.715, about twice that for B_4C. The icosahedra do not break during the shear to the large strain of 0.802.

To understand these structural transformation mechanisms, we examined its relation to the bonding changes for $(B_{11}C_p)-Si_2$; Figures 3 and 4 show the structures and the isoelectron surface (at 0.9) from the electron localization function (ELF) analysis at various critical strains. The ELF, which ranges from 0 to 1, enables an effective and reliable analysis of covalent bonding and lone pair formation.[35,36]

Figure 3 shows the first structural transition to another stable conformation. Figure 3a shows the intact structure where the icosahedron has 25 electrons for intraicosahedral bonding, one less than Wade's rule because each Si makes four 2c−2e bonds. As the strain increases to 0.245 that corresponds to maximum stress of 30.4 GPa, the B−C bonds between icosahedra increase by 20% to 1.997 Å, as shown in Figure 3b. Continuous shear to 0.263 strain leads to the stress drops through breaking B−C bond between cages, as shown in Figure 3c. The electron counting scheme at 0.263 strain changes and the cage has 27 electrons. As the strain increases to 0.314 (Figure 3d), the Si−Si bond in the chain breaks and the Si atoms rebond to the unbonded B and C atoms in the cage. Now the cage has 25 electrons again. As the strain increase to 0.397 (Figure 3e), another stable structure forms where one Si connects to three boron atoms in cages and the other Si connects to two boron and one carbon atoms in cages. This new stable structure is slightly lower in energy by 7.9 kcal/mol per icosahedron.

Figure 4 shows the second structural transition where the new structure recovers to its original structure. Figure 4a shows the structure that corresponds to the second maximum stress at 0.689 strain. The B−B bonds between cages are stretched to 2.18 Å. As the shear increases to 0.715, the Si−Si chain bonds and B−B bonds between cages break and the Si rebonds to the unbonded boron atom in the cage, as shown in Figure 4b. Continuous shear to 0.741 leads to the reformation of Si−Si chain bond and B−B bond between cages, as shown in Figure 4c,d. It is worth noticing that the electron counting scheme does not changes during the second structural transition.

There is, of course, a practical problem in synthesizing this $(B_{11}C_p)-Si_2$ material. How do we ensure that the Si does not go inside the icosahedron and the C and B do not go into the chain? Experimental synthesis from various starting materials involves complex transformations well beyond the QM methods used here. However, the theory can help by predicting signatures for the atoms being at various locations. For example, the QM calculated NMR chemical shifts for $(B_{11}C_p)-Si_2$ are 86.4 ppm for C_p and 457.3 and 475.6 ppm for Si, whereas for $(B_{11}Si)$-CSi they are 36.2 ppm for C_{chain}, 464.2 ppm for Si_{chain}, and 814.8 ppm for Si_{cage}, respectively. Thus, by measuring XPS, XANES, NMR, Raman, and IR for

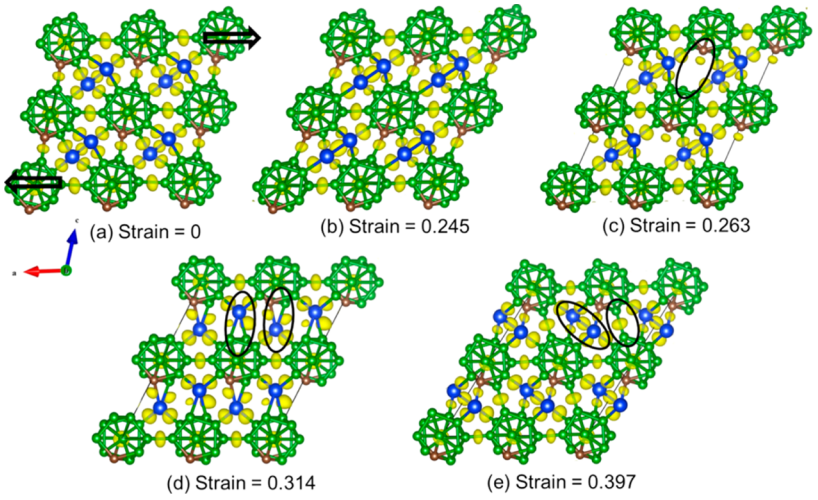

Figure 3. $(B_{11}C_p)-Si_2$ structures and ELF of the first structural transition shearing along $(01\bar{1}1)/<\bar{1}101>$ amorphous slip system of B_4C: (a) the intact structure; (b) the structure corresponds to the maximum stress where the B−C bond distance between icosahedra increases by 20% to 1.997 Å, point A in Figure 2; (c) the structure where the B−C bonds between icosahedra break, point B in Figure 2; (d) the structure where the Si−Si bonds in the chain break and the Si atoms rebond to the unbonded B, C atoms from previous breaking B−C bond, point C in Figure 2; and (e) the transformed structure with new formed Si−Si bond and B−B bond between icosahedra, point D in Figure 2

dx.doi.org/10.1021/jz5022697 | J. Phys. Chem. Lett. 2014, 5, 4169−4174

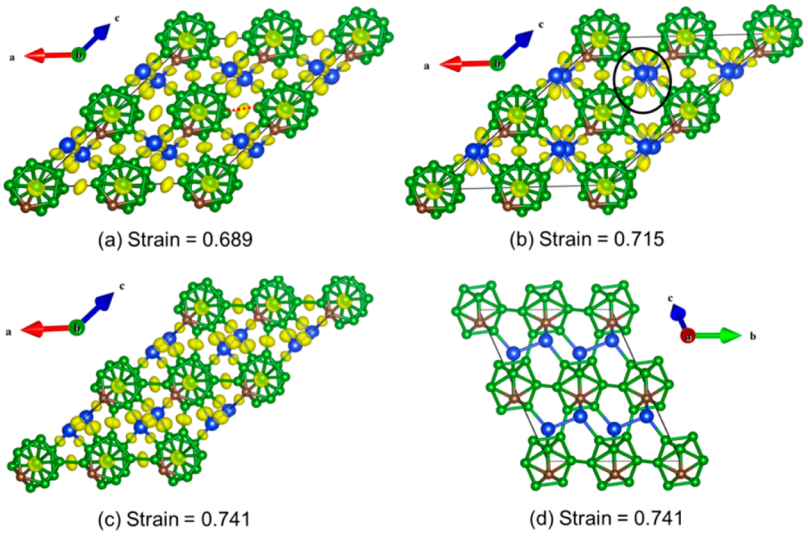

Figure 4. $(B_{11}C_p)$−Si_2 structures and ELF of the second structural transition shearing along $(01\bar{1}\bar{1})/<\bar{1}101>$ amorphous slip system of B_4C: (a) the structure corresponds to the second maximum stress and the B−B bond between cages (red dashed line) is stretched to 2.18 Å, point E in Figure 2; (b) the structure where the Si−Si chain bonds and B−B cage bonds break and Si rebonds to the unbonded boron atoms in the cage, point F in Figure 2; (c) the second structural transition where the Si−Si chain bond and B−B cage bonds reform, point G in Figure 2; and (d) the same structure as (c), but viewed along "a" direction that clearly shows the reformation of Si−Si chain bond.

samples prepared under various synthesis conditions, we might be able to select conditions that favor $(B_{11}C_p)$−Si_2 by comparing to the predicted signatures for each distribution in the experiment.

In summary, we show that mechanical properties can change dramatically as we modify the CBC chain in the $(B_{11}C_p)$CBC structure. In particular, replacing the CBC chain with the Si−Si pair dramatically increases the ductility of the boron carbide. Moreover, the density decreases by 2.7%, while the hardness decreases by only 12%.

COMPUTATIONAL METHODS

All DFT calculations were performed using the VASP package,[37−39] with Perdew−Burke−Ernzerhof (PBE) functional and the projector-augmented wave method to account for the core−valence interactions.[40] We found that a kinetic energy cutoff of 600 eV for the plane-wave expansions gives excellent convergence of the total energies, energy differences, and structural parameters. Reciprocal space was sampled using the Γ-centered Monkhorst−Pack scheme with a resolution less than $2\pi \times 1/40$ Å^{-1}. The convergence criteria were set to 1×10^{-6} eV energy difference for solving for the electronic wave function and 1×10^{-3} eV/Å force for geometry optimization.

To establish the stability of the predicted crystal structure, we calculated the Hessian and phonon modes using the supercell approach with finite displacements, as implemented in PHONPY code.[41]

To make a preliminary estimate of ductility, we used the Paugh criterion[34] that high values of B/G (particularly B/G > 1.75) are more ductile, where B is the bulk modulus and G is the shear modulus. We first computed the elastic constant C_{ij} from the stress−strain relation as a function of various cell distortions from the equilibrium lattice configuration.[42] Then, the inverse of the elasticity tensor S_{ij} was derived from $S_{ij} = (C_{ij})^{-1}$. Finally, we used the Voigt−Reuss−Hill (VRH) approximation[43] to calculate the isotropic polycrystalline elastic moduli from the corresponding single-crystal elastic constants. The VRH average is the arithmetic mean of the Voigt and Reuss bounds. For Voigt average, the bulk modulus, B_V, and shear modulus, G_V, are expressed as

$$B_V = (C_{11} + C_{22} + C_{33} + 2C_{12} + 2C_{13} + 2C_{23})/9$$

and

$$G_V = (C_{11} + C_{22} + C_{33} - C_{12} - C_{13} - C_{23} + 3C_{44} + 3C_{55} + 3C_{66})/15$$

For Reuss average, the bulk modulus, B_R, and shear modulus, G_R, are expressed as

$$B_R = 1/(S_{11} + S_{22} + S_{33} + 2S_{12} + 2S_{13} + 2S_{23})$$

and

$$G_R = 15/(4S_{11} + 4S_{22} + 4S_{33} - 4S_{12} - 4S_{13} - 4S_{23} + 3S_{44} + 3S_{55} + 3S_{66})$$

We also computed the Knoop hardness based on the electronegativity, covalent radii of the constituent atoms, and the bond lengths in the structure.[44,45]

To examine the shear failure of the modified materials, we imposed the strain for a particular shear plane, while allowing full structure relaxation of the atoms and of the other five strain components.[46] The residual stresses after relaxing these other strain directions were <0.5 GPa. For these shear simulations, we used supercells varying from 112 atoms to 120 atoms, and the Monkhorst−Pack grid $(3 \times 3 \times 3)$ in the k-space was used.

AUTHOR INFORMATION

Corresponding Author

*E-mail: wag@wag.caltech.edu.

Notes

The authors declare no competing financial interest.

ACKNOWLEDGMENTS

We thank Dr. Sergey Zybin and Dr. Andres Jaramillo-Botero at Caltech for the useful discussions. This work was supported by

the Defense Advanced Research Projects Agency (W31P4Q-13-1-0010, program manager, Judah Goldwasser). The computers used in these studies were provided by NSF-CSEM and ONR-DURIP grants. The crystal structure was drawn using the VESTA software.[47]

REFERENCES

(1) Haines, J.; Léger, J. M.; Bocquillon, G. Synthesis and Design of Superhard Materials. *Annu. Rev. Mater. Res.* **2001**, *31*, 1−23.
(2) Riedel, R. Novel Ultrahard Materials. *Adv. Mater.* **1994**, *6*, 549−560.
(3) Veprek, S.; Zeer, A.; Riedel, R. *Handbook of Ceramic Hard Materials*; Wiley-VCH Press: Weinheim, Germany, 2000.
(4) An, Q.; Goddard, W. A., III; Xiao, H.; Cheng, T. Deformation Induced Solid−Solid Phase Transitions in Gamma Boron. *Chem. Mater.* **2014**, *26*, 4289−4298.
(5) Brazhkin, V. V. High-Pressure Synthesized Materials: Treasures and Hints. *High Pressure Res.* **2007**, *27*, 333−351.
(6) Ivanovskii, A. L. Mechanical and Electronic Properties of Diborides of Transition 3d−5d Metals from First Principles: Toward Search of Novel Ultra-incompressible and Superhard Materials. *Prog. Mater. Sci.* **2012**, *57*, 184−228.
(7) Zhao, Y. S.; Qian, J.; Daemen, L. L.; Pantea, C.; Zhang, J. Z.; Voronin, G. A.; Zerda, T. W. Enhancement of Fracture Toughness in Nanostructured Diamond−SiC Composites. *Appl. Phys. Lett.* **2004**, *84*, 1356−1358.
(8) Sigl, L. S.; Mataga, P. A.; Dalgleish, B. J.; McMeeking, R. M.; Evans, A. G. On the Toughening of Brittle Materials Reinforced with a Ductile Phase. *Acta Metall.* **1988**, *36*, 945−953.
(9) Fang, Z. Z.; Griffo, A.; White, B.; Lockwood, G.; Belnap, D.; Hilmas, G.; Bitler, J. Fracture Resistant Super Hard Materials and Hardmetals Composite with Functionally Designed Microstructure. *Int. J. Refract. Metals Hard Met.* **2001**, *19*, 453−459.
(10) Reddy, K. M.; Guo, J. J.; Shinoda, Y.; Fujita, T.; Hirata, A.; Singh, J. P.; McCauley, J. W.; Chen, M. W. Enhanced Mechanical Properties of Nanocrystalline Boron Carbide by Nanoporosity and Interface Phases. *Nat. Commun.* **2012**, *3*, 1052.
(11) Sezer, A. O.; Brand, J. I. Chemical Vapor Deposition of Boron Carbide. *Mater. Sci. Eng., B* **2001**, *79*, 191−202.
(12) Thevenot, F. Boron Carbide—A Comprehensive Review. *J. Eur. Ceram. Soc.* **1990**, *6*, 205−225.
(13) Domnich, V.; Reynaud, S.; Haber, R. A.; Chhowalla, M. Boron Carbide: Structure, Properties, and Stability under Stress. *J. Am. Ceram. Soc.* **2011**, *94*, 3605−3628.
(14) Hoard, J. L.; Hughes, R. E. *The Chemistry of Boron and Its Compounds*; Wiley: New York, 1967.
(15) Suri, A. K.; Subramanian, C.; Sonber, J. K.; Murthy, T. Synthesis and Consolidation of Boron Carbide: A Review. *Int. Mater. Rev.* **2010**, *55*, 4−40.
(16) Chen, M. W.; McCauley, J. W.; Hemker, K. J. Shock-Induced Localized Amorphization in Boron Carbide. *Science* **2003**, *299*, 1563−1566.
(17) Fanchini, G.; McCauley, J. W.; Chhowalla, M. Behavior of Disordered Boron Carbide under Stress. *Phys. Rev. Lett.* **2006**, *97*, 035502.
(18) Yan, X. Q.; Tang, Z.; Zhang, L.; Guo, J. J.; Jin, C. Q.; Zhang, Y.; Goto, T.; McCauley, J. W.; Chen, M. W. Depressurization Amorphization of Single-Crystal Boron Carbide. *Phys. Rev. Lett.* **2009**, *102*, 075505.
(19) Shirai, K. Electronic Structures and Mechanical Properties of Boron and Boron-Bich Crystals (Part I). *J. Superhard Mater.* **2010**, *32*, 205−225.
(20) Shirai, K. Electronic Structures and Mechanical Properties of Boron and Boron-Bich Crystals (Part II). *J. Superhard Mater.* **2010**, *32*, 336−345.
(21) Emin, D. Unusual Properties of Icosahedral Boron-Rich Solids. *J. Solid State Chem.* **2006**, *179*, 2791−2798.
(22) Bourne, N. K. Shock−induced Brittle Failure of Boron Carbide. *Proc. R. Soc. London, Ser. A* **2002**, *458*, 1999−2006.
(23) Johnson, G. R.; Holmquist, T. J. Response of Boron Carbide Subjected to Large Strains, High Strain Rates, and High Pressures. *J. Appl. Phys.* **1999**, *85*, 8060−8073.
(24) Mashimo, T.; Uchino, M. Heterogeneous Free-surface Profile of B_4C Polycrystal under Shock Compression. *J. Appl. Phys.* **1997**, *81*, 7064−7066.
(25) Vogler, T. J.; Reinhart, W. D.; Chhabildas, L. C. Dynamic Behavior of Boron Carbide. *J. Appl. Phys.* **2004**, *95*, 4173−4183.
(26) Domnich, V.; Gogotsi, Y.; Trenary, M.; Tanaka, T. Nano-indentation and Raman Spectroscopy Studies of Boron Carbide. *Appl. Phys. Lett.* **2002**, *81*, 3783−3785.
(27) Yan, X. Q.; Li, W. J.; Goto, T.; Chen, M. W. Raman Spectroscopy of Pressure-induced Amorphous Boron Carbide. *Appl. Phys. Lett.* **2006**, *88*, 131905.
(28) Chen, M. W.; McCauley, J. W. Mechanical Scratching Induced Phase Transitions and Reactions of Boron Carbide. *J. Appl. Phys.* **2006**, *100*, 123517.
(29) Reddy, K. M.; Liu, P.; Hirata, A.; Fujita, T.; Chen, M. W. Atomic Structure of Amorphous Shear Bands in Boron Carbide. *Nat. Commun.* **2013**, *4*, 2483.
(30) An, Q.; Goddard, W. A., III; Cheng, T. Atomistic Explanation of Shear-induced Amorphous Band Formation in Boron Carbide. *Phys. Rev. Lett.* **2014**, *113*, 095501.
(31) Matkovich, V. I. Interstitial Compounds of Boron. *J. Am. Chem. Soc.* **1961**, *83*, 1804−1806.
(32) Wade, K. The Structural Significance of the Number of Skeletal Bonding Electron-pairs in Carboranes, the Higher Boranes and Borane Anions, and Various Transition-metal Carbonyl Cluster Compounds. *J. Chem. Soc. D* **1971**, *15*, 792−793.
(33) Mingos, D. M. P. A General Theory for Cluster and Ring Compounds of the Main Group and Transition Elements. *Nat. Phys. Sci.* **1972**, *236*, 99−102.
(34) Pugh, S. F. Relations between the Elastic Moduli and the Plastic Properties of Polycrystalline Pure Metals. *Philos. Mag.* **1954**, *45*, 823−843.
(35) Becke, A. D.; Edgecombe, K. E. A Simple Measure of Electron Localization in Atomic and Molecular Systems. *J. Chem. Phys.* **1990**, *92*, 5397−5403.
(36) Silvi, B.; Savin, A. Classification of Chemical Bonds Based on Topological Analysis of Electron Localization Functions. *Nature (London)* **1994**, *371*, 683−686.
(37) Kresse, G.; Hafner, J. Ab Initio Molecular Dynamics for Liquid Metals. *Phys. Rev. B* **1993**, *47*, 558−561.
(38) Kresse, G.; Furthmuller, J. Efficiency of Ab-Initio Total Energy Calculations for Metals and Semiconductors Using a Plane-Wave Basis Set. *Comput. Mater. Sci.* **1996**, *6*, 15−50.
(39) Kresse, G.; Furthmüller, J. Efficient Iterative Schemes for Ab Initio Total-Energy Calculations Using a Plane-Wave Basis Set. *Phys. Rev. B* **1996**, *16*, 11169−11186.
(40) Kresse, G.; Joubert, D. From Ultrasoft Pseudopotentials to the Projector Augmented-Wave Method. *Phys. Rev. B* **1999**, *59*, 1758−1775.
(41) Togo, A.; Oba, F.; Tanaka, I. First-Principles Calculations of the Ferroelastic Transition between Rutile-Type and $CaCl_2$-Type SiO_2 at High Pressures. *Phys. Rev. B* **2008**, *78*, 134106.
(42) Le Page, Y.; Saxe, P. Symmetry-general Least-squares Extraction of Elastic Data for Strained Materials from Ab Initio Calculations of Stress. *Phys. Rev. B* **2002**, *65*, 104104.
(43) Hill, R. The Elastic Behaviour of a Crystalline Aggregate. *Proc. Phys. Soc., London, Sect. A* **1952**, *65*, 349−354.
(44) Li, K. Y.; Wang, X. T.; Zhang, F. F.; Xue, D. F. Electronegativity Identification of Novel Superhard Materials. *Phys. Rev. Lett.* **2008**, *100*, 235504.
(45) Lyakhov, A. O.; Oganov, A. R. Evolutionary Search for Superhard Materials: Methodology and Applications to Forms of Carbon and TiO2. *Phys. Rev. B* **2011**, *84*, 092103.

(46) Roundy, D.; Krenn, C. R.; Cohen, M. L.; Morris, J. W., Jr. Ideal Shear Strengths of fcc Aluminum and Copper. *Phys. Rev. Lett.* **1999**, *82*, 2713−2716.
(47) Momma, K.; Izumi, F. VESTA 3 for Three-dimensional Visualization of Crystal, Volumetric and Morphology Data. *J. Appl. Crystallogr.* **2011**, *44*, 1272−1276.